Stem Cell Reports
Article

ISSCR

OPEN ACCESS

Tubastatin A maintains adult skeletal muscle stem cells in a quiescent state *ex vivo* and improves their engraftment ability *in vivo*

Marina Arjona,[1,2] Armon Goshayeshi,[1,2,5] Cristina Rodriguez-Mateo,[1,2,5] Jamie O. Brett,[1,2,3,5] Pieter Both,[1,2,3] Heather Ishak,[1,2] and Thomas A. Rando[1,2,4,*]

[1]Department of Neurology and Neurological Sciences, Stanford University School of Medicine, Stanford, CA, USA
[2]Glenn Center for the Biology of Aging, Stanford University School of Medicine, Stanford, CA, USA
[3]Stem Cell Biology and Regenerative Medicine Graduate Program, Stanford University School of Medicine, Stanford, CA, USA
[4]Neurology Service, Veterans Affairs Palo Alto Health Care System, Palo Alto, CA, USA
[5]These authors contributed equally
*Correspondence: rando@stanford.edu
https://doi.org/10.1016/j.stemcr.2021.11.012

SUMMARY

Adult skeletal muscle stem cells (MuSCs) are important for muscle regeneration and constitute a potential source of cell therapy. However, upon isolation, MuSCs rapidly exit quiescence and lose transplantation potency. Maintenance of the quiescent state *in vitro* preserves MuSC transplantation efficiency and provides an opportunity to study the biology of quiescence. Here we show that Tubastatin A (TubA), an Hdac6 inhibitor, prevents primary cilium resorption, maintains quiescence, and enhances MuSC survival *ex vivo*. Phenotypic characterization and transcriptomic analysis of TubA-treated cells revealed that TubA maintains most of the biological features and molecular signatures of quiescence. Furthermore, TubA-treated MuSCs showed improved engraftment ability upon transplantation. TubA also induced a return to quiescence and improved engraftment of cycling MuSCs, revealing a potentially expanded application for MuSC therapeutics. Altogether, these studies demonstrate the ability of TubA to maintain MuSC quiescence *ex vivo* and to enhance the therapeutic potential of MuSCs and their progeny.

INTRODUCTION

Skeletal muscle is characterized by a remarkable regenerative capacity mediated by tissue-specific muscle stem cells (MuSCs) (Dhawan and Rando, 2005; Schmidt et al., 2019). MuSCs reside under the muscle fiber basal lamina and are distinguished by the expression of the transcription factor Pax7 (Mauro, 1961; Seale et al., 2000). Under physiological conditions, MuSCs persist in a state of quiescence, but they become activated in response to different types of stress or injury (Cheung and Rando, 2013). Following activation, MuSCs enter the cell cycle and rapidly proliferate to produce myogenic progenitor cells that either differentiate into mature myofibers or self-renew and return to a quiescent state, preserving the MuSC pool (Motohashi and Asakura, 2014; Olguin and Olwin, 2004).

Quiescence is a reversible state characterized by cell-cycle arrest in which cells retain the ability to respond to different signals from their environment and re-enter the cell cycle (Cheung and Rando, 2013; van Velthoven and Rando, 2019). Quiescent cells exhibit enhanced resistance to several stresses, increased autophagic activity, small cell size, low protein synthesis, low total RNA content, and low turnover (Gray et al., 2004; Valcourt et al., 2012; van Velthoven and Rando, 2019). Quiescent MuSCs are distinguished by the expression of different myogenic regulatory factors, low transcriptional activity, and low expression of proliferation markers (Fukada et al., 2007; Olguin and Olwin, 2004; van Velthoven and Rando, 2019).

As soon as MuSCs are isolated and grown in conventional culture conditions *ex vivo*, they quickly activate out of quiescence and undergo cell division (Montarras, 2005). Important changes in intracellular trafficking and signaling, metabolic pathways, and gene expression are observed during MuSC exit out of quiescence, resulting in profound molecular alterations. Therefore, the ability to maintain stem cells in a quiescent state *in vitro* would significantly enhance the ability to study the biology of quiescence and the mechanisms that govern this state (Quarta et al., 2016). Simultaneously, a better characterization of MuSC quiescence would allow the development of novel approaches to improve homeostasis and repair of damaged or diseased muscle.

Another important potential application of maintaining cultured MuSCs in a quiescent state includes the ability to perform *ex vivo* gene editing for stem cell-based gene therapy. Additionally, a promising therapeutic strategy to treat many muscle diseases and traumatic injuries is the transplantation of MuSCs (Rinaldi and Perlingeiro, 2014). After transplantation, MuSCs are able to divide and either contribute to new myonuclei in growing myofibers or repopulate the stem cell compartment (Judson and Rossi, 2020). However, *ex vivo* expansion of MuSCs not only results in a loss of stemness but also in a considerable loss of their regenerative potential and reduction of engraftment ability (Montarras, 2005). Therefore, the ability to improve the engraftment potential of MuSCs that have been expanded *in vitro* is required to significantly enhance their therapeutic efficiency (Quarta et al., 2016).

Many types of quiescent cells exhibit a primary cilium, which is a microtubule-based organelle, anchored at the cellular membrane (Tucker et al., 1979a). A major function of the primary cilium is to integrate and transduce extracellular signals and to coordinate intracellular signaling pathways. One of the most important developmental pathways regulated by this organelle is the Hedgehog (Hh) signaling pathway (Anvarian et al., 2019; Huangfu et al., 2003). Primary cilia assembly and disassembly are intimately linked to cell cycle progression, with the primary cilia beginning to disassemble as cells enter the cell cycle (Kim and Tsiokas, 2011; Quarmby and Parker, 2005; Tucker et al., 1979b). The histone deacetylase 6 (Hdac6) plays a crucial role in promoting ciliary resorption by inducing the deacetylation of axonemal microtubules (de Diego et al., 2014; Pugacheva et al., 2007).

The primary cilium is present at the surface of MuSCs during quiescence but disassembles upon MuSC activation out of quiescence and entry into the cell cycle (Jaafar Marican et al., 2016). Ablation of primary cilia in adult MuSCs causes impaired muscle regeneration, lower engraftment capacity, and increased expression of cell-cycle-related genes (Palla et al., 2020). Furthermore, it has been described that repression of Hh signaling by the primary cilium is important in maintaining MuSCs in a quiescent state (Betania Cruz-Migoni et al., 2019; Palla et al., 2020). Activation of Hh signaling triggers MuSC activation and proliferation (Betania Cruz-Migoni et al., 2019; Palla et al., 2020).

Because Hdac6 appears to be an important mediator of ciliary resorption, the regulation of either Hdac6 expression or activity has been previously used to modulate ciliary dynamics and signaling, which in turn modulate cellular proliferation and, in the setting of cancer, tumor growth (Gradilone et al., 2013; Pugacheva et al., 2007; Rao et al., 2014). Tubastatin A (TubA) has been recently developed as a potent and specific small-molecule inhibitor of Hdac6 (Butler et al., 2010). Indeed, Hdac6 inhibition by TubA has been shown to increase primary cilium formation in different cell lines, and to decrease cellular proliferation *in vitro* and to reduce tumor growth *in vivo* (Gradilone et al., 2013; Pham et al., 2019; Rao et al., 2014; Tao et al., 2018; Woan et al., 2015). These findings show that TubA can be used as a powerful and effective tool to control both primary cilium dynamics and cell cycle progression.

Here we show that TubA prevents MuSC activation and progression into the cell cycle and preserves the typical phenotypic and transcriptomic characteristics of quiescent cells. Our results show that TubA, through its Hdac6 inhibitory function, impedes primary cilium resorption in quiescent MuSCs *ex vivo*, and that TubA improves MuSC engraftment potential in transplantation studies. Furthermore, TubA is able to induce a return to quiescence and improve the transplantation efficiency of cycling MuSCs, revealing a potentially valuable approach to enhancing the therapeutic potential of MuSCs.

RESULTS

TubA prevents MuSC entry into the cell cycle

It has been described that the primary cilium is present in quiescent MuSCs but disassembles as soon as MuSCs exit out of quiescence and that the presence of the primary cilium induces the repression of Hh signaling and maintenance of the quiescence state (Betania Cruz-Migoni et al., 2019; Jaafar Marican et al., 2016; Palla et al., 2020). Furthermore, TubA has been shown to increase primary cilium formation and to downregulate Hh signaling (Gradilone et al., 2013). Based on these studies, we wondered whether TubA could maintain MuSCs in a quiescent state *ex vivo* by inhibiting primary cilium resorption and thus repressing Hh signaling. To investigate this, we first examined the effects of TubA on MuSC activation ability. Freshly isolated MuSCs ($MuSCs^{FI}$) are characterized by reduced cell size, low RNA content, low cellular metabolism, and decreased protein synthesis, exhibiting typical characteristics of quiescent cells (van Velthoven and Rando, 2019). We cultured $MuSCs^{FI}$ in the presence of different doses of TubA for up to 120 h. Entry into the cell cycle was measured by EdU (5-ethynyl-2′-deoxyuridine) incorporation. At the highest dose tested (40 μM), TubA prevented almost 100% of the cells from exiting quiescence, and this effect was sustained up to 120 h (Figure 1A).

In order to test if this effect was reversible, we treated $MuSCs^{FI}$ with 40 μM of TubA for 120 h and then washed TubA out and maintained the cells for 40 h in the presence of EdU (Figure 1B). We found that release from TubA allowed the cells to activate and incorporate EdU similarly to vehicle-treated MuSCs ($MuSCs^{Veh}$) exiting from quiescence. These functional studies show that TubA is able to maintain isolated MuSCs in a state of reversible quiescence for extended periods of time.

TubA prevents FAP entry into the cell cycle

In order to determine whether the effects of TubA were specific to MuSCs, we tested the effects of TubA on fibroadipogenic progenitors (FAPs). Freshly isolated FAPs were cultured in the presence of increasing doses of TubA for up to 48 h (Figure S1A). We found that 20 μM of TubA was enough to block EdU incorporation in almost 100% of FAPs. Similar to MuSCs, FAPs were able to activate and incorporate EdU after being released from TubA (Figure S1B). Altogether, these results demonstrate the ability of TubA to prevent entry into the cell cycle of multiple cell types.

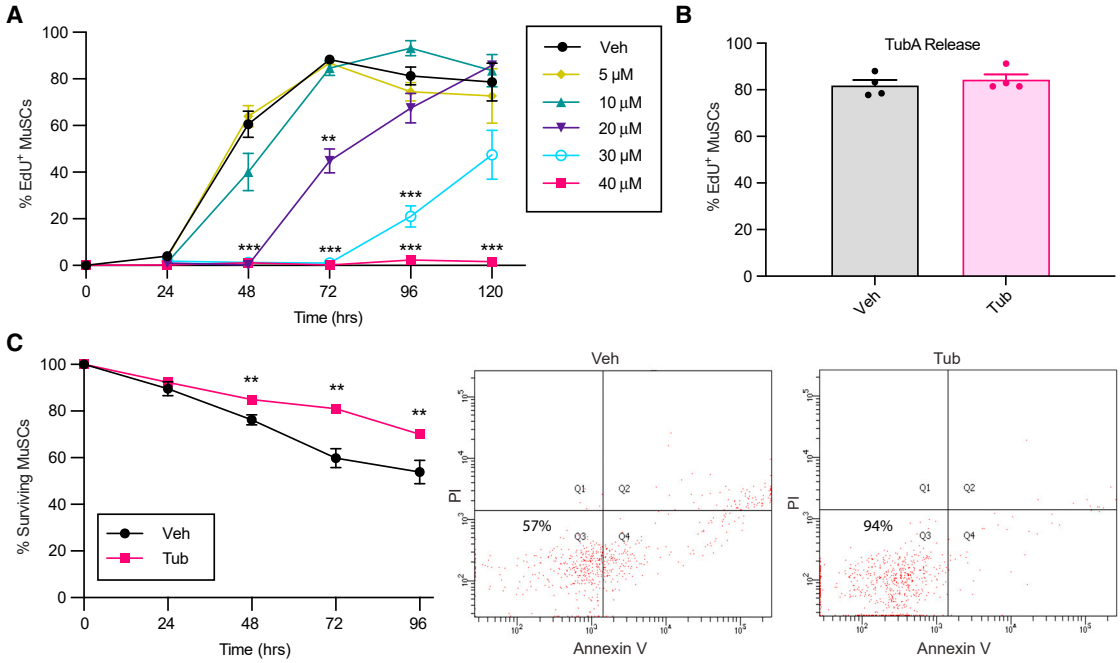

Figure 1. TubA prevents MuSC entry into the cell cycle and enhances MuSC survival

(A) MuSCs^{FI} were treated with different doses of TubA while being cultured continuously in EdU to assess S-phase progression. Cells were fixed at different time points, and the percentage of EdU+ MuSCs was quantified (n = 8 mice in Veh and 40 µM TubA; n = 4 mice in other conditions).

(B) MuSCs were treated with vehicle (Veh) or with 40 µM of TubA for 120 h (Tub). Cells were then cultured for 40 h in absence of TubA but the presence of EdU, after which the number of MuSCs+ for EdU was quantified (n = 4 mice).

(C) MuSCs^{FI} were cultured for different periods of times in the absence or presence of 40 µM of TubA and then stained with Annexin V and propidium iodide (PI) to determine viability by flow cytometry. Shown are the quantification of the fraction of surviving cells at the different time points (left) and representative FACS plots (right) at 72 h with indicated survival percentages (n = 8 mice). Error bars represent ±s.e.m. **p < 0.01, ***p < 0.001; no asterisk: not significant; two-tailed paired t test.

TubA improves MuSC survival

Adult stem cells maintained in a quiescent state *in vivo* exhibit a remarkable ability to withstand environmental stress (Cheung and Rando, 2013; Der Vartanian et al., 2019; Scaramozza et al., 2019). However, in conventional *ex vivo* culture conditions, the absence of signals derived from the niche leads to considerable MuSC death (Liu et al., 2018; White et al., 2018). We therefore wondered whether TubA, by sustaining quiescence, would improve cell viability in isolated MuSCs over time. To test this, we cultured MuSCs^{FI} in the presence of 40 µM TubA for up to 96 h and analyzed the cultures for cell death by Annexin V staining. TubA significantly reduced the percentage of MuSCs succumbing to apoptotic cell death over time (Figure 1C). These findings demonstrate the ability of TubA to reduce apoptotic cell death in MuSCs cultured *ex vivo*.

TubA prevents MuSC activation

Because TubA was able to prevent cell cycle entry of MuSCs^{FI}, we sought to further characterize the phenotypic features of TubA-treated MuSCs (MuSCs^{Tub}). We studied the behavior of MuSCs^{Veh} during the process of activation compared with MuSCs^{Tub} maintained in culture for the same amount of time. Cell growth is one of the first processes that occurs upon MuSC activation and was measured by using fluorescence-activated cell sorting (FACS) and analyzing forward scatter area (FSC-A) (Brett et al., 2020). We found that, after 72 h in culture, MuSCs^{Tub} were much smaller than MuSCs^{Veh} (Figure 2A). We confirmed this result by assessing cell size using a Coulter counter. Whereas MuSCs^{Veh} increased in size over time, MuSCs^{Tub} remained small and exhibited negligible growth up to 72 h in culture (Figure 2B). Another feature of MuSC activation is an increase in RNA content (Dell'Orso et al., 2019; Tang and Rando, 2014). We found that, whereas total RNA content increased by over two-fold in MuSCs^{Veh} over 72 h in culture, no increase was observed in MuSCs^{Tub} (Figure 2C). The MuSC-specific transcription factor Pax7 is highly expressed in quiescence but downregulated as MuSCs activate out of quiescence and enter the cell cycle (Seale et al., 2000) (Figure 2D). We found that TubA maintains Pax7 expression at significant higher levels compared

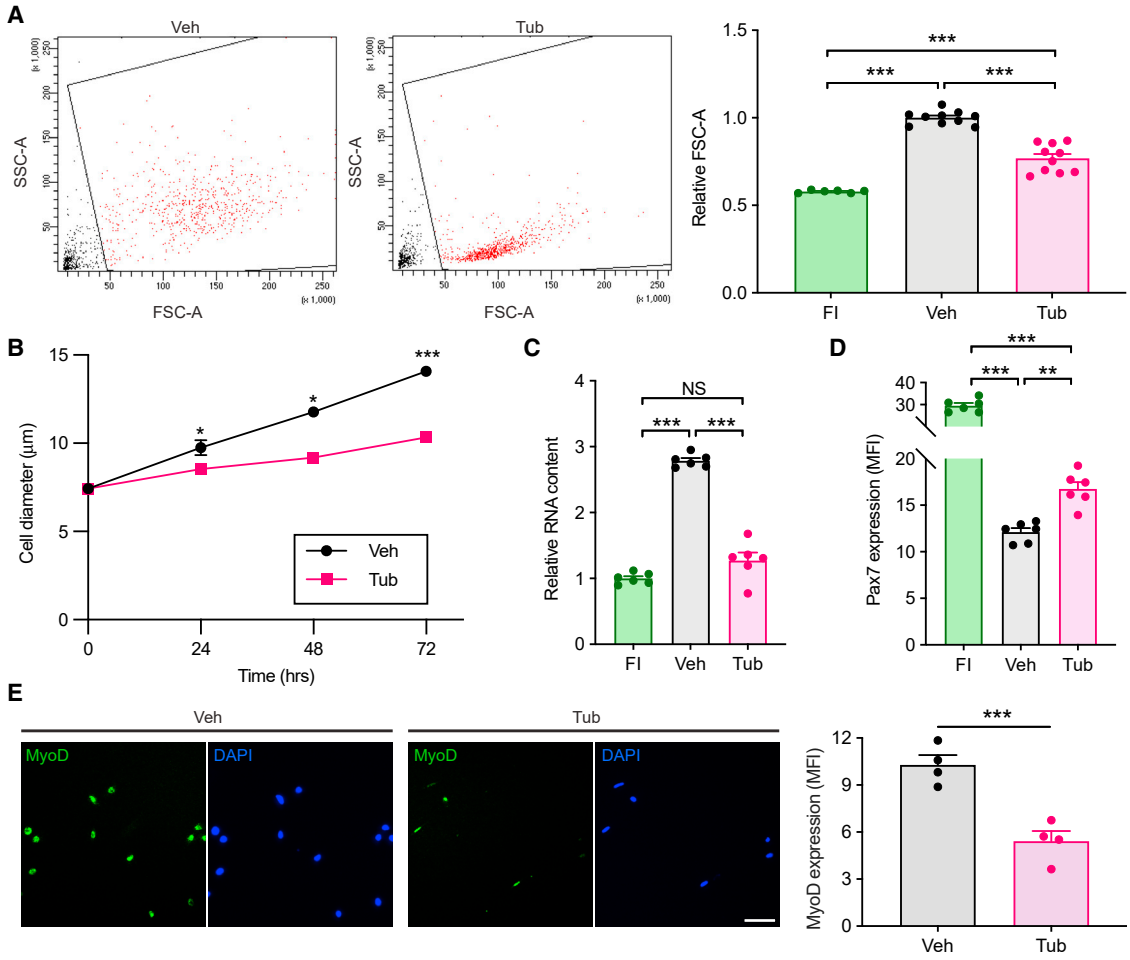

Figure 2. TubA-treated cells exhibit typical phenotypic attributes of quiescent MuSCs

MuSCs^{FI} were cultured in the presence (Tub) or absence (Veh) of 40 μM of TubA for 72 h.

(A) Cells were analyzed for cellular size by flow cytometry based on forward scatter area (FSC-A). Representative FACS plots (left) and a graph with relative FSC-A values (right) are shown. Data were normalized to the mean level in MuSCs^{Veh} (n = 10 mice in Veh and Tub; n = 6 mice in FI).

(B) Cell size was measured with a Coulter counter at 0, 24, 48, or 72 h (n = 12 mice at 0 h, n = 10 mice at 24 and 48 h, and n = 4 mice at 72 h).

(C) Cells were assayed for RNA content based on Pyronin Y intensity in flow cytometry. Data were normalized to the mean level in MuSCs^{FI} (n = 6 mice).

(D) FACS-isolated MuSCs were cultured for 72 h and then analyzed for Pax7 expression by immunofluorescence. Shown is the quantification of Pax7 mean fluorescence intensity (MFI) in MuSCs^{FI}, MuSCs^{Veh}, and MuSCs^{Tub} (n = 6 mice).

(E) MyoD immunofluorescence of either MuSCs^{Veh} or MuSCs^{Tub} fixed after 72 h. Representative images are shown on the left. Quantification of MyoD mean fluorescence intensity (MFI) is shown on the right (n = 4 mice). Scale bar in e, 50 μm. Error bars represent ±s.e.m. *p < 0.05, **p < 0.01, ***p < 0.001; two-tailed paired t test in (A)–(E).

with MuSCs^{Veh} after 72 h in culture (Figure 2D). However, Pax7 expression levels were reduced by 50% in MuSCs^{Tub} compared with those of MuSCs^{FI} (Figure 2D). We then analyzed MyoD, a master regulator of myogenic differentiation known to start being expressed at the protein level soon after MuSCs activate out of quiescence (de Morrée et al., 2017; Hausburg et al., 2015). Compared with MuSCs^{Veh}, MuSCs^{Tub} exhibited significantly less MyoD protein expression up to 72 h in culture (Figure 2E). These data indicate that MuSCs^{Tub} exhibit typical phenotypic attributes of quiescent MuSCs. Taken together, these experiments show that TubA prevents MuSC activation and maintains the typical features of quiescence in MuSCs grown *ex vivo* for up to 72 h.

TubA decreases MuSC primary cilium resorption

Previous findings suggest an important role of the primary cilium in MuSCs by regulating their exit from quiescence

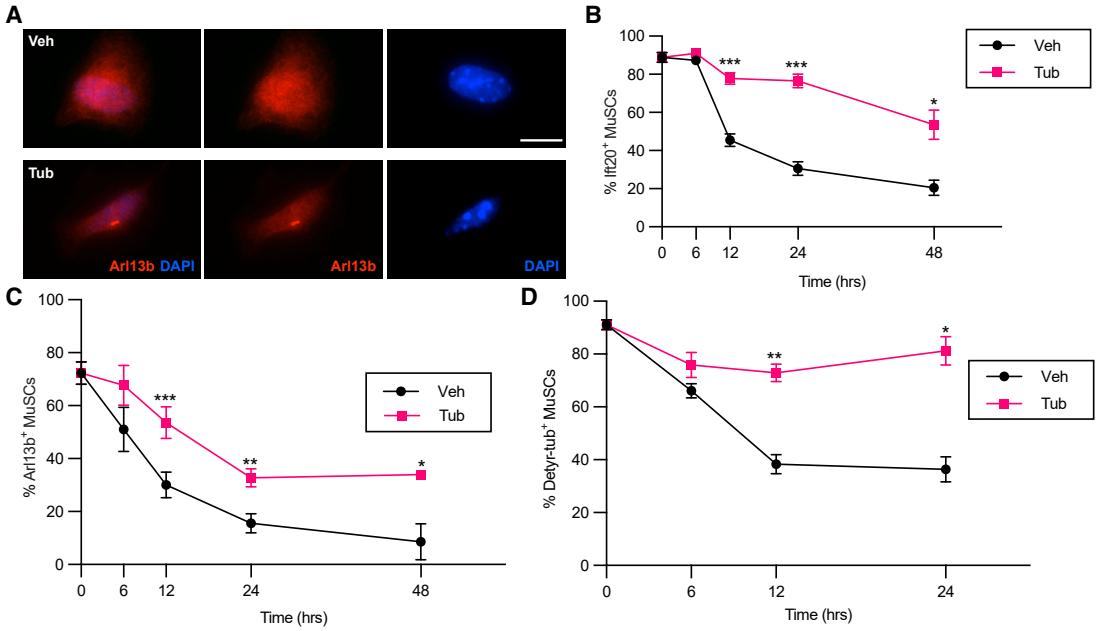

Figure 3. TubA maintains a higher proportion of ciliated MuSCs

(A–C) MuSCs^{FI} were cultured in the presence or absence of 40 μM of TubA and fixed and stained for primary cilium markers at 0, 6, 12, 24, and 48 h. (A) Representative images of MuSCs^{Veh} and MuSCs^{Tub} cultured for 48 h and stained for Arl13b and DAPI. (B) MuSCs were assayed for Ift20 expression based on immunocytochemistry (n = 8 mice at 0, 12, and 24 h; n = 4 mice at 6 and 48 h). (C) MuSCs were stained for Arl13b by immunocytochemistry (n = 8 mice at 0, 12 and 24 h; n = 4 mice at 6 and 48 h).

(D) MuSCs^{FI} were cultured in the presence or absence of 40 μM of TubA and fixed and stained for detyrosinated tubulin (Detyr-tub) at 0, 6, 12, and 24 h (n = 4 mice). Scale bar in (A), 10 μm. Error bars represent ±s.e.m. *p < 0.05, **p < 0.01, ***p < 0.001; no asterisk: not significant; two-tailed paired t test in (B)–(D).

and controlling MuSC proliferation and differentiation (Betania Cruz-Migoni et al., 2019; Palla et al., 2020). Hdac6 has been proposed to facilitate primary cilium resorption (de Diego et al., 2014; Pugacheva et al., 2007), and its inhibition by TubA has been shown to restore the formation of primary cilia and to decrease cell proliferation in different cell lines (Gradilone et al., 2013; Rao et al., 2014). Consequently, we hypothesized that treatment of MuSCs with TubA *ex vivo* would hinder the resorption of the primary cilium associated with MuSC activation. To test this, we treated MuSCs with TubA and examined the cells for the presence of the primary cilium by immunofluorescence. To visualize this organelle, we used antibodies directed against intraflagellar transport protein 20 (Ift20) and ADP-ribosylation factor-like 13b (Arl13b), both of which are involved in cilia assembly and maintenance (Caspary et al., 2007; Follit et al., 2006), and an antibody directed against detyrosinated tubulin, a posttranslational modification involved in the anterograde intraflagellar transport (Follit et al., 2006; Sirajuddin et al., 2014). Ift20 is localized to both the basal body and the primary cilium, whereas Arl13b, a small guanosine triphosphatase, is localized to the ciliary membrane (Caspary et al., 2007; Follit et al., 2006). Detyrosinated tubulin is enriched on the outer doublets B tubules of the axonemal microtubules (Johnson, 1998). We found that TubA treatment was able to maintain a higher proportion of ciliated MuSCs (exhibiting Ift20, Arl13b, and detyrosinated tubulin staining) compared with MuSCs^{Veh} after being cultured *ex vivo* (Figures 3A–3D). Thus, these experiments indicate that TubA inhibits the resorption of the primary cilium in conventional *ex vivo* MuSC culture conditions.

TubA-treated MuSCs exhibit a quiescent transcriptome signature

To examine the state of quiescence preserved by TubA at the transcriptome level, we performed RNA-seq on MuSCs^{Veh} or MuSCs^{Tub} after being cultured for 24 h, as well as on freshly isolated cells for comparison. Principal component analysis (PCA) of all expressed genes revealed a higher correlation of the transcriptome of MuSCs^{Tub} with the transcriptome of MuSCs^{FI} than that of MuSCs^{Veh} (Figure 4A). We found that 2,572 genes were similarly expressed between MuSCs^{FI} and MuSCs^{Tub} (Benjamini-Hochberg-corrected p value >0.05, fold-change <2). Specifically, of these 2,572 similarly expressed genes, 1,266 genes were significantly different in MuSCs^{Veh} compared with MuSCs^{FI} (FDR 1%, fold-change ≥4). To examine potential

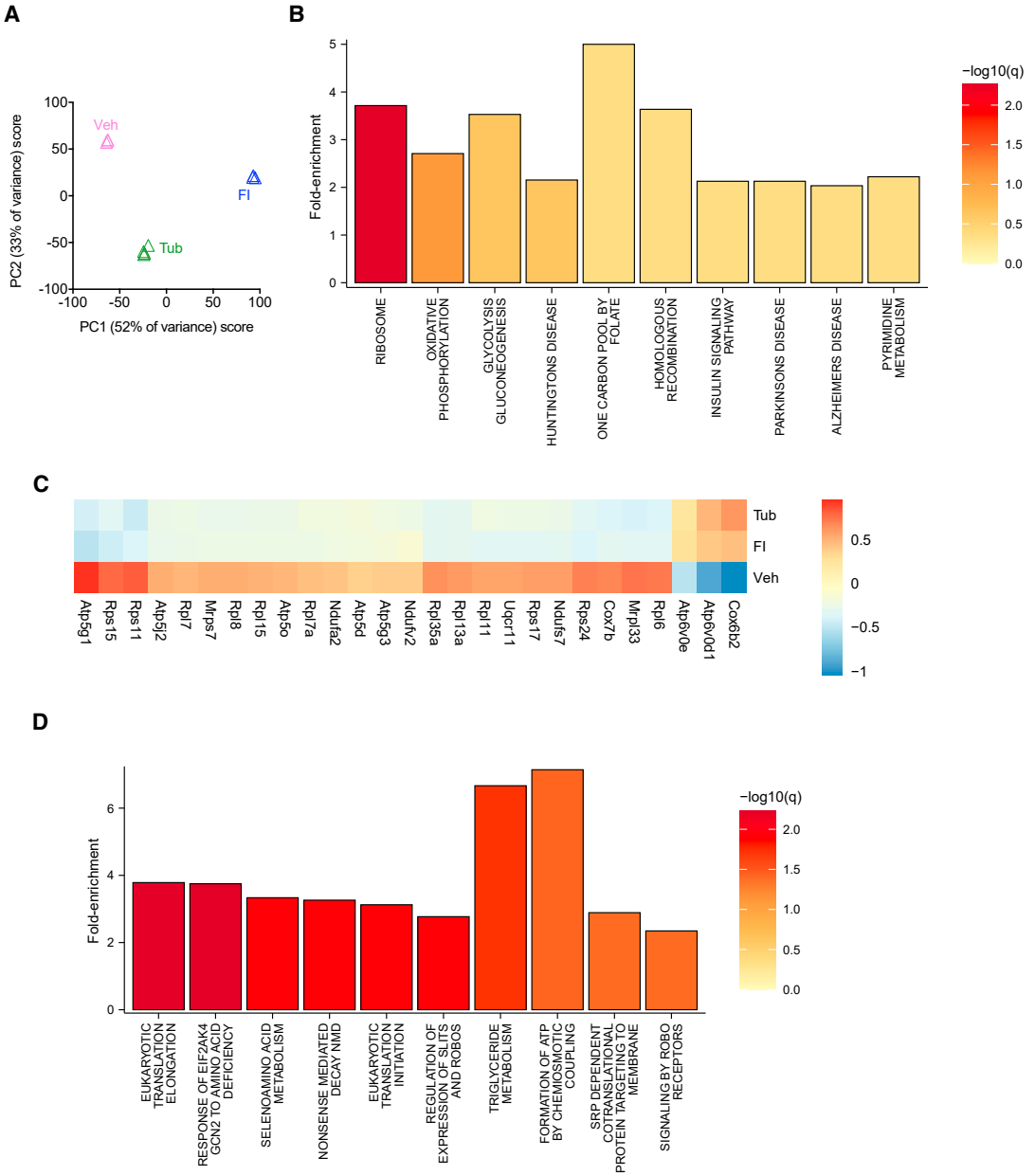

Figure 4. Similarities between the transcriptomes of MuSCs^{Tub} and MuSCs^{FI}

(A) PCA of RNA-seq profiles of MuSCs^{FI}, and of MuSCs^{Veh}, or MuSCs^{Tub} cultured for 24 h. Each profile represents the MuSCs of an individual mouse (n = 3 mice for MuSCs^{FI}, n = 3 mice for MuSCs^{Veh}, and n = 4 mice for MuSCs^{Tub}).

(B) Summary plot for the over-representation analysis using the KEGG database. Over-represented signaling pathways of the similarly expressed genes between MuSCs^{FI} and MuSCs^{Tub} are shown.

(C) Heatmap of similarly expressed genes between the MuSCs^{FI} and the MuSCs^{Tub} transcriptomes but differentially expressed in the MuSCs^{Veh}.

(D) Summary plot for the over-representation analysis using the REACTOME gene set collection. Over-represented signaling pathways of the similarly expressed genes between MuSCs^{FI} and MuSCs^{Tub} are shown.

pathways involved in the maintenance of quiescence by TubA, we performed over-representation analysis using the KEGG gene set collection (Kanehisa, 2000). The top hits of this analysis were ribosome- and oxidative phosphorylation-related genes (Figures 4B and 4C). To further characterize these TubA-regulated genes, we used the

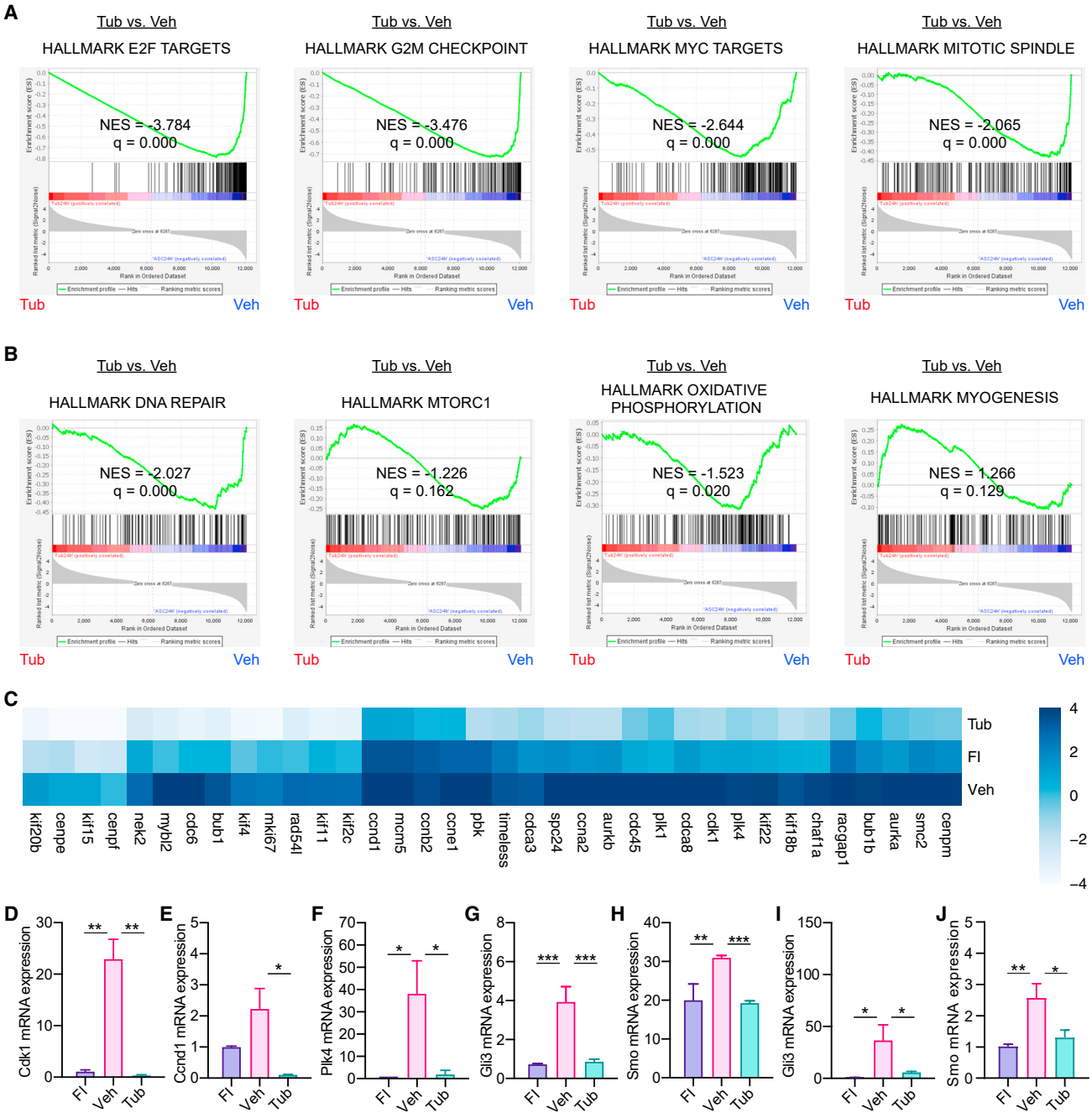

Figure 5. Transcriptional differences between MuSCs^{Tub} and MuSCs^{Veh}

(A and B) GSEA results for the Hallmark gene sets in comparisons of RNA-seq profiles for MuSCs^{Tub} versus MuSCs^{Veh} after being cultured for 24 h. (A) GSEA enrichment plots for the E2F targets gene set, the G2/M checkpoint gene set, the Myc targets gene set, and the mitotic spindle gene set are shown. (B) GSEA enrichment plots for the DNA repair gene set, the mTORC gene set, the oxidative phosphorylation gene set, and the myogenesis gene set.

(C) Heatmap of differentially expressed genes between the MuSCs^{Tub} and the MuSCs^{Veh} transcriptomes.

(D–F) RT-qPCR analyses were done in MuSCs^{FI}, and in MuSCs^{Veh} and MuSCs^{Tub} after being cultured for 24 h. C_t values were normalized first to the mean of *Gapdh* and then to the mean of MuSCs^{FI} level in each experiment. RT-qPCR analysis of Cdk1 in (D), Ccnd1 in (E), and Plk4 in (F) (n = 3 mice).

(legend continued on next page)

REACTOME gene set collection (Jassal et al., 2019). We found an enrichment in transcripts involved in translation and ATP synthesis (Figure 4D), which correlated with the findings from the KEGG gene set collection. Furthermore, metabolism-related gene sets such as triglyceride metabolism, selenoamino acid metabolism, and metabolism of water-soluble vitamins and cofactors were also found to be enriched using the REACTOME gene set collection (Figure 4D).

To investigate the molecular mechanisms underlying the effects of TubA on MuSCs in more detail, we examined the transcriptional differences between $MuSCs^{Tub}$ and $MuSCs^{Veh}$ in the RNA-seq data. We performed gene set enrichment analysis (GSEA) using the Hallmark gene set collection (Subramanian et al., 2005). Compared with $MuSCs^{Veh}$, $MuSCs^{Tub}$ exhibited different expression levels of cell-cycle-promoting signaling gene sets including E2F targets, G2/M checkpoint, Myc targets, and mitotic spindle gene sets (Figure 5A). Furthermore, GSEA revealed that DNA repair, mTORC1 signaling, metabolism-related (cholesterol homeostasis, oxidative phosphorylation, and fatty acid metabolism), and myogenesis factors were among the differentially expressed gene sets (Figure 5B). Most of the cell-cycle-promoting signaling genes consisted of centrosome, microtubule, and primary cilium associated proteins involved in cell cycle regulation (Figure 5C). We performed RT-qPCR to validate the changes for select genes implicated in cell cycle progression and centriole duplication and found that the expression levels of some of these genes, such as Cdk1, Ccnd1, and Plk4, were lower in $MuSCs^{Tub}$ compared with $MuSCs^{Veh}$, confirming the results obtained in the RNA-seq analysis (Figures 5D–5F).

Because activation of ciliary-mediated Hh signaling has been associated with MuSC exit from quiescence and entry into the cell cycle (Betania Cruz-Migoni et al., 2019; Palla et al., 2020), we then analyzed the expression of Hh signaling genes in our RNA-seq data. We found an upregulation of Smo and Gli3 expression in $MuSCs^{Veh}$ (Figures 5G and 5H), as has been previously shown (Betania Cruz-Migoni et al., 2019; Palla et al., 2020). However, the expression of these specific genes in $MuSCs^{Tub}$ was similar to the expression levels in quiescent $MuSCs^{FI}$ (Figures 5G and 5H). These results were then confirmed by RT-qPCR analysis (Figures 5I and 5J). Ptch1 mRNA was nearly undetectable in both RNA-seq and RT-qPCR assays. These findings, together with the low expression levels of cell-cycle-related genes in response to TubA treatment, suggest that the ability of TubA in holding MuSCs in a quiescent state *ex vivo* could be due to the maintenance of the primary cilium and the subsequent repression of Hh signaling preventing MuSC entry into the cell cycle.

TubA improves MuSC engraftment ability

Because of their important role in muscle repair and regeneration (Lepper et al., 2011; Relaix and Zammit, 2012; Sambasivan et al., 2011), MuSCs have been considered as potential sources of cell therapy for muscle injury and for the treatment of muscular dystrophies (Collins et al., 2005; Sacco et al., 2008; Webster et al., 2016). After being transplanted into damaged or diseased muscles, MuSCs are able to expand and fuse with host myofibers (Collins et al., 2005; Sacco et al., 2008; Webster et al., 2016). However, MuSCs rapidly lose engraftment and regenerative potential as they activate out of quiescence when expanded in culture prior to transplantation (Gilbert et al., 2010; Ikemoto et al., 2007; Montarras, 2005; Quarta and Rando, 2015). Because MuSCs maintain a quiescent phenotype when cultured in the presence of TubA, we sought to determine whether TubA treatment would improve the engraftment potential of MuSCs in transplantation experiments. In order to test this, we used, as donors, $Pax7^{CreER}$; $R26R^{RFP}$ mice, which express RFP specifically in adult MuSCs after tamoxifen administration. Freshly isolated RFP+ MuSCs were cultured in the presence of TubA for 72 h and transplanted into injured tibialis anterior (TA) muscles of NSG mice. Ten days later, the TAs were collected and analyzed. We found that TubA significantly increased the total number of RFP+ muscle fibers relative to control (Figure 6A), suggesting that TubA enhances the regenerative potential of MuSCs maintained *in vitro*. Indeed, no differences in the number of RFP+ fibers were observed between transplanted $MuSCs^{FI}$ and $MuSCs^{Tub}$ (Figure 6A).

We then tested the effect of TubA treatment on MuSC survival immediately after transplantation. MuSCs that expressed a luciferase reporter were treated with TubA for 72 h and then transplanted into recipient NSG mice. Bioluminescence (BLI) analysis 24 h after transplantation showed that BLI signal from $MuSCs^{Tub}$ was significantly higher than that of $MuSCs^{Veh}$ but comparable to that of $MuSCs^{FI}$ (Figure 6B), suggesting similar survival rates between 72-h-treated $MuSCs^{Tub}$ and quiescent MuSCs. Next, we investigated the *in vivo* proliferation rate of MuSC populations after transplantation. Non-invasive imaging for seven days showed comparable expansions of $MuSCs^{Tub}$ and

(G and H) mRNA expression levels of Hh signaling genes such as Gli3 (G) and Smo (H) in $MuSCs^{FI}$ and in $MuSCs^{Veh}$ and $MuSCs^{Tub}$ after being cultured for 24 h. Data obtained from our RNA-seq analysis ($n = 3$ mice for $MuSCs^{FI}$, $n = 3$ mice for $MuSCs^{Veh}$, and $n = 4$ mice for $MuSCs^{Tub}$). (I and J) RT-qPCR analysis of either Gli3 (I) or Smo (J) in MuSCs. C_t values were normalized first to the mean of *Gapdh* and then to the mean of $MuSCs^{FI}$ level in each experiment ($n = 6$ mice). NES, normalized enrichment score in (A) and (B). Error bars represent ±s.e.m. *$p < 0.05$, **$p < 0.01$, ***$p < 0.001$; no asterisk: not significant; one-tailed t test in (D)–(J).

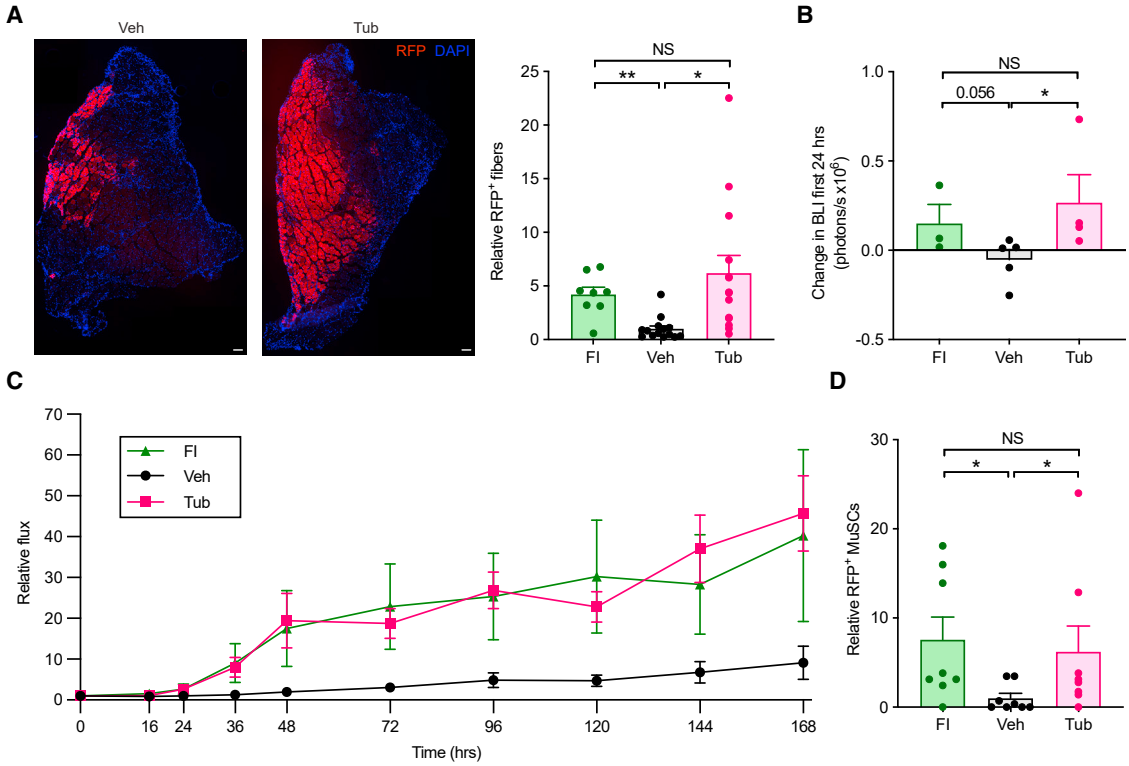

Figure 6. TubA treatment enhances the regenerative potential of MuSCs maintained *in vitro*

(A) FACS-isolated MuSCs from *Pax7*^{CreER}; *R26R*^{RFP} donor mice were cultured in the presence or absence of 40 μM of TubA for 72 h and then transplanted into injured tibialis anterior (TA) muscles of NSG mice. We injected MuSCs^{Tub} in one leg of a given mouse and MuSCs^{Veh} in the contralateral leg of that same mouse. MuSCs^{FI} were isolated from *Pax7*^{CreER}; *R26R*^{RFP} mice and transplanted into injured TA muscles of recipient mice as a control. Ten days after transplantation, TA muscles were collected, sectioned, and assayed for RFP+ myofibers by immunohistochemistry. DAPI was used to stain nuclei. Representative images of TA muscles transplanted with either MuSCs^{Veh} or MuSCs^{Tub} are shown on the left. Quantification of the number of RFP+ fibers in TA muscles transplanted with either MuSCs^{FI}, MuSCs^{Veh}, or MuSCs^{Tub} is shown on the right. Data were normalized to the mean level in MuSCs^{Veh} (n = 14 mice in Veh and Tub; n = 8 mice in FI).

(B and C) FACS-isolated MuSCs that express a luciferase reporter were cultured in the presence or absence of 40 μM of TubA for 72 h and then transplanted into injured TA muscles of NSG mice. MuSCs^{Tub} were injected in one leg of a given mouse and MuSCs^{Veh} in the contralateral leg of that same mouse. MuSCs^{FI} were transplanted into injured TA muscles of recipient mice as a control. (B) Bioluminescence analysis was done at 0 and 24 h after transplantation. The bioluminescence signal obtained at 0 h (baseline bioluminescence signal) was then subtracted from that obtained at 24 h, and the results from this calculation are shown (n = 5 mice in Veh; n = 4 mice in Tub; n = 3 mice in FI). (C) Transplanted mice were assayed for bioluminescence for 168 h. Data were normalized to the mean level at 0 h (n = 5 mice in Veh; n = 4 mice in Tub; n = 3 mice in FI).

(D) FACS-isolated MuSCs from *Pax7*^{CreER}; *R26R*^{RFP} donor mice were cultured in the presence or absence of 40 μM of TubA for 72 h and then transplanted into injured TA muscles of NSG mice. We injected MuSCs^{Tub} in one leg of a given mouse and MuSCs^{Veh} in the contralateral leg of that same mouse. MuSCs^{FI} were isolated from *Pax7*^{CreER}; *R26R*^{RFP} mice and transplanted into injured TA muscles of recipient mice as a control. Four weeks after transplantation, TA muscles were collected, sectioned, and assayed for RFP+ MuSCs by immunohistochemistry. The total number of RFP+ MuSCs in TA muscles transplanted with either MuSCs^{FI}, MuSCs^{Veh}, or MuSCs^{Tub} was quantified. Data were normalized to the mean level at MuSCs^{Veh} (n = 8 mice). Scale bar in (A), 100 μm. Error bars represent ± SEM. *p < 0.05, **p < 0.01; NS: not significant; two-tailed paired t test in (A)–(D).

MuSCs^{FI} but a much lower rate of expansion of MuSCs^{Veh} (Figure 6C). To test whether, following TubA treatment and subsequent withdrawal, the progeny of the treated cells behave as the progeny of MuSCs^{FI} do, we compared the *in vitro* proliferation rate as well as the differentiation potential of MuSCs^{Tub} following their release from TubA treatment with those of MuSCs^{FI} cultured *ex vivo*. We found that the *in vitro* proliferation and differentiation characteristics of progeny of MuSCs^{Tub} and MuSCs^{FI} were indistinguishable (Figures S2A and S2B).

To determine to which extent TubA treatment preserves MuSC self-renewal capacity, RFP+ MuSCs isolated from

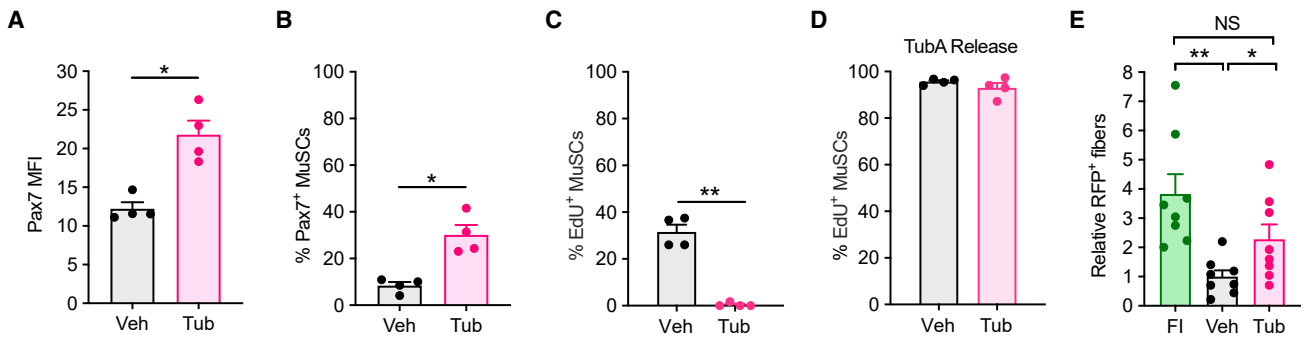

Figure 7. TubA induces re-quiescence in cycling MuSCs

(A–C) MuSCs^{FI} were grown for 72 h and then cultured in the presence or absence of 40 μM of TubA for 48 h. EdU was added to the cells 15 min before fixation. MuSCs were stained for Pax7 by immunocytochemistry. Pax7 mean fluorescence intensity (MFI) (A), the number of Pax7+ cells (B), and the percentage of EdU+ cells (C) were quantified (n = 4 mice).

(D) MuSCs^{FI} were expanded in culture for 72 h and then cultured in the presence or absence of 40 μM of TubA for 48 h. Cells were then cultured for 48 h in the absence of TubA but the presence of EdU, after which the number of EdU+ MuSCs was quantified (n = 4 mice).

(E) FACS-isolated MuSCs from *Pax7^{CreER}; R26R^{RFP}* donor mice were grown for 72 h and then treated with or without 40 μM of TubA for 48 h. These cells were then transplanted into injured TA muscles of NSG mice. We injected MuSCs^{Tub} in one leg of a given mouse and MuSCs^{Veh} in the contralateral leg of that same mouse. MuSCs^{FI} were isolated from *Pax7^{CreER}; R26R^{RFP}* mice and transplanted into injured TA muscles of recipient mice as a control. Ten days after transplantation, TA muscles were collected, sectioned, and assayed for RFP+ myofibers by immunohistochemistry. DAPI was used to stain nuclei. The total number of RFP+ fibers in TA muscles transplanted with either MuSCs^{FI}, MuSCs^{Veh}, or MuSCs^{Tub} was quantified. Data were normalized to the mean level at MuSCs^{Veh} (n = 8 mice). Error bars represent ± s.e.m. *p < 0.05, **p < 0.01; no asterisk: not significant; two-tailed paired t test.

Pax7^{CreER}; R26R^{RFP} mice were cultured in the presence of TubA for 72 h and then transplanted into previously injured TA muscles of NSG mice. Four weeks after transplantation, the TA muscles were collected and the numbers of RFP+ MuSCs were quantified. The number of self-renewed MuSCs obtained from the transplantation of MuSCs^{Tub} was significantly higher than that from transplantation of MuSCs^{Veh} but comparable to that following MuSC^{FI} transplantation (Figure 6D), indicating that maintenance of a quiescent state by TubA treatment preserves MuSC potency and allows efficient self-renewal ability *in vivo*.

TubA induces re-quiescence in activated MuSCs

Given the rarity of MuSCs following isolation from muscle samples, the expansion of these cells *in vitro* is required to obtain enough cells for cellular therapy (Charville et al., 2015; Judson and Rossi, 2020). However, as noted, *in vitro* expansion of MuSCs results in a marked reduction in transplantation efficacy compared with freshly isolated cells (Montarras, 2005). To explore if TubA could induce a return to quiescence of MuSCs that had already activated and begun to proliferate, we allowed MuSCs to expand in culture for 72 h and then treated them with TubA for 48 h. We found that TubA induced Pax7 expression and decreased the number of cycling MuSCs as measured by EdU incorporation (Figures 7A–7C). To confirm that the non-cycling cells were indeed in a state of quiescence, we washed out TubA and maintained the cells in culture for an additional 48 h in the presence of EdU (Figure 7D). We found that the cells then entered into the cell cycle similarly to control cells. These experiments show that TubA addition to cycling MuSCs induces their return to a quiescent state.

We therefore wondered whether TubA, by inducing a return to quiescence, would improve the transplantation ability of *ex vivo* expanded MuSCs. To investigate this, freshly isolated, RFP+ MuSCs were expanded in culture for 72 h and then treated with TubA for 48 h. These cells were then transplanted into previously injured TA muscles of NSG mice. Ten days after transplantation, the TA muscles were collected and the numbers of RFP+ fibers were quantified. TubA treatment significantly increased the number of RFP+ fibers relative to vehicle treatment (Figure 7E). Indeed, MuSCs^{Tub} yielded similar numbers of RFP+ fibers as did MuSCs^{FI} (Figure 7E). These findings suggest that TubA could be used for cellular therapy by improving the transplantation efficacy of *in vitro* expanded MuSCs.

DISCUSSION

Here we provide evidence that TubA is able to prevent MuSCs from activation and progression into S-phase. Further characterization of MuSCs^{Tub} revealed features typical of quiescent cells, such as small cell size, low RNA content, low expression levels of myogenic differentiation

factors, and enhanced resilience. Transcriptomic analysis of MuSCs^{Tub} also revealed patterns typical of quiescent cells, further demonstrating the ability of TubA to maintain MuSCs in a quiescent state *ex vivo* and to enhance their regenerative potential in transplantation experiments. Additionally, TubA treatment was able to induce re-quiescence and improve the transplantation efficacy of activated MuSCs.

Our experiments show that TubA impedes primary cilium resorption in quiescent MuSCs and maintains low expression levels of centrosome, microtubule, and primary cilium-related genes, including Cdk1/Cyclin B, AurkA, and NEK2, involved in cell cycle regulation. By coordinating centriole duplication and mitotic spindle apparatus formation, these cell-cycle-related proteins control the balance between ciliary assembly and disassembly. Cdk1/Cyclin B inhibits Plk4-induced centriole duplication, AurkA starts the disassembly of the primary cilium by activating Hdac6, and NEK2 facilitates ciliary disassembly by activating kinesins (Hong et al., 2015; Pugacheva et al., 2007; Zitouni et al., 2016). Low expression levels of each of these genes in response to TubA treatment ensure both the maintenance of the primary cilium in MuSCs cultured *ex vivo* and the persistence of the ciliary repression on mitogenic signaling. Additionally, given the strong association of the primary cilium with Hh signaling and the importance of Hh signaling in MuSC exit from quiescence (Betania Cruz-Migoni et al., 2019; Palla et al., 2020), the preservation of quiescent expression levels of Hh signaling genes by TubA conditions could be contributing to the preservation of MuSC quiescence. Indeed, our results reveal that TubA promotes primary cilium formation and decreases cell proliferation in MuSCs. These findings are in accordance with recent studies showing decreased cellular proliferation after TubA treatment in various cellular types, such as melanoma cells, cholangiocarcinoma cells, and esophageal cancer cell lines (Gradilone et al., 2013; Tao et al., 2018; Woan et al., 2015). The effects of TubA treatment on the primary cilium could be associated with the maintenance of MuSC quiescence; however, this association has not yet been causally demonstrated. Further experiments need to be done in order to test this causal relationship.

MuSCs constitute an important cellular source for muscle therapy in the context of muscle injury or in the treatment of muscular dystrophies (Webster et al., 2016). However, as soon as MuSCs are isolated and cultured in conventional conditions *ex vivo*, they rapidly exit quiescence, activate, and proliferate, losing their stem cell potency (Ikemoto et al., 2007; Montarras, 2005; Quarta and Rando, 2015). The ability of TubA to induce a return to quiescence of cycling MuSCs, enhancing MuSC potential for cellular therapy after their expansion *in vitro*, demonstrates the importance of TubA applicability, constituting a potential valuable and effective tool in the context of muscle cell therapeutics.

EXPERIMENTAL PROCEDURES

Detailed methods can be found in the supplemental experimental procedures.

Animals

Animals were housed in pathogen-free rooms and maintained with a 12-h light-dark cycle in the Veterinary Medical Unit at the Veterans Affairs Palo Alto Health Care System. Animal protocols and care were approved by the Institutional Animal Care and Use Committee. Two- to three-month-old C57BL/6J mice (strain 000664) and *R26R^{RFP}* mice on the C57BL/6J background (strain 007914) were purchased from The Jackson Laboratory. Two- to three-month-old FVB-Tg(CAG-luc,-GFP)L2G85Chco/J (strain 008450) male mice and NOD.Cg-Prkdcscid Il2rgtm1Wjl/SzJ (strain 005557) male mice were obtained from Jackson Laboratory. *Pax7^{CreER}* mice are on the C57BL/6 x 129/SvJ background (Brack et al., 2007). Pax7^{CreER}; Rosa26R^{RFP} were generated by mating *Pax7^{CreER}* and *R26R^{RFP}* mice. Two- to four-month-old Pax7^{CreER}; Rosa26R^{RFP} male mice were used for transplantation experiments.

Cellular purification by FACS

MuSC isolation protocol was performed as previously described (Liu et al., 2015). Hindlimb and triceps muscles were finely chopped with scissors and digested in Collagenase II and Dispase (Invitrogen). A 20G needle was used to dissociate MuSCs from myofibers, and the resulting solution was filtered using a 40-μm cell strainer and labeled with specific antibodies. MuSCs were then purified by surface antigen-based isolation (CD31- CD45- Sca1- VCAM+). In transplantation experiments, RFP-based isolation was used to purify MuSCs. Aria II and Aria III machines (BD Biosciences) were used to obtain pure MuSC populations. In order to check the purity of the MuSC population collected, an aliquot of cells was stained with Pax7 antibodies (1:50, DSHB AB_528428). FAPs were also purified by surface antigen-based isolation (CD31- CD45- Sca1+ VCAM-).

MuSC culture and treatment with Tubastatin A

Purified MuSCs were immediately plated on glass chamber slides coated with poly-D-lysine (0.1 mg/mL, EMD Millipore) and extracellular matrix (ECM, 25 μg/mL, Sigma) for immunofluorescence assays, or on plastic tissue-culture plates coated with ECM for all other experiments. *Ex vivo* culture of MuSCs was performed in wash media (Ham's F-10 media containing 10% horse serum, 100 U/mL penicillin, and 100 μg/mL streptomycin). Tubastatin A (Cayman Chemical) was dissolved in DMSO and, unless otherwise indicated, used at a concentration of 40 μM. An equal volume of DMSO was added to control cells.

Data and code availability

The data that support the findings of this study are available from the corresponding author upon request. RNA-seq data have been deposited in the NCBI Gene Expression Omnibus.The accession

number for the RNA-seq data reported in this paper is GEO: GSE178070.

SUPPLEMENTAL INFORMATION

Supplemental information can be found online at https://doi.org/10.1016/j.stemcr.2021.11.012.

AUTHOR CONTRIBUTIONS

M.A. and T.A.R. designed experiments. M.A., A.G., C.R-M., J.O.B., P.B., and H.I. conducted and analyzed experiments. M.A. and T.A.R. wrote the manuscript.

CONFLICT OF INTERESTS

The authors declare no conflict of interest.

ACKNOWLEDGMENTS

We thank all the people in the Rando Lab for intellectual support.

This research was funded by grants from the Stanford University School of Medicine Medical Scientist Training Program (T32 GM007365) to J.O.B. and from the NIH (P01 AG036695 and R01 AR062185) and the Department of Veterans Affairs (Merit Review) to T.A.R.

Received: June 15, 2021
Revised: November 24, 2021
Accepted: November 25, 2021
Published: December 30, 2021

REFERENCES

Anvarian, Z., Mykytyn, K., Mukhopadhyay, S., Pedersen, L.B., and Christensen, S.T. (2019). Cellular signalling by primary cilia in development, organ function and disease. Nat. Rev. Nephrol. *15*, 199–219.

Betania Cruz-Migoni, S., Imran, K.M., Wahid, A., Rahman, O., Briscoe, J., and Borycki, A.-G. (2019). A switch in cilia-mediated Hedgehog signaling controls muscle stem cell quiescence and cell cycle progression. bioRxiv https://doi.org/10.1101/2019.12.21.884601.

Brack, A.S., Conboy, M.J., Roy, S., Lee, M., Kuo, C.J., Keller, C., and Rando, T.A. (2007). Increased Wnt signaling during aging alters muscle stem cell fate and increases fibrosis. Science *317*, 807–810.

Brett, J.O., Arjona, M., Ikeda, M., Quarta, M., de Morrée, A., Egner, I.M., Perandini, L.A., Ishak, H.D., Goshayeshi, A., Benjamin, D.I., et al. (2020). Exercise rejuvenates quiescent skeletal muscle stem cells in old mice through restoration of Cyclin D1. Nat. Metab. *2*, 307–317.

Butler, K.V., Kalin, J., Brochier, C., Vistoli, G., Langley, B., and Kozikowski, A.P. (2010). Rational design and simple chemistry yield a superior, neuroprotective HDAC6 inhibitor, tubastatin A. J. Am. Chem. Soc. *132*, 10842–10846.

Caspary, T., Larkins, C.E., and Anderson, K.V. (2007). The graded response to sonic Hedgehog depends on cilia architecture. Dev. Cell *12*, 767–778.

Charville, G.W., Cheung, T.H., Yoo, B., Santos, P.J., Lee, G.K., Shrager, J.B., and Rando, T.A. (2015). Ex vivo expansion and in vivo self-renewal of human muscle stem cells. Stem Cell Reports *5*, 621–632.

Cheung, T.H., and Rando, T.A. (2013). Molecular regulation of stem cell quiescence. Nat. Rev. Mol. Cell Biol. *14*, 329–340.

Collins, C.A., Olsen, I., Zammit, P.S., Heslop, L., Petrie, A., Partridge, T.A., and Morgan, J.E. (2005). Stem cell function, self-renewal, and behavioral heterogeneity of cells from the adult muscle satellite cell niche. Cell *122*, 289–301.

Dell'Orso, S., Juan, A.H., Ko, K.-D., Naz, F., Perovanovic, J., Gutierrez-Cruz, G., Feng, X., and Sartorelli, V. (2019). Single cell analysis of adult mouse skeletal muscle stem cells in homeostatic and regenerative conditions. Development *146*, dev174177.

Dhawan, J., and Rando, T.A. (2005). Stem cells in postnatal myogenesis: molecular mechanisms of satellite cell quiescence, activation and replenishment. Trends Cell Biol. *15*, 666–673.

de Diego, A.S., Alonso Guerrero, A., Martínez-A, C., and van Wely, K.H.M. (2014). Dido3-dependent HDAC6 targeting controls cilium size. Nat. Commun. *5*, 3500.

Follit, J.A., Tuft, R.A., Fogarty, K.E., and Pazour, G.J. (2006). The intraflagellar transport protein IFT20 is associated with the golgi complex and is required for cilia assembly. Mol. Biol. Cell *17*, 3781–3792.

Fukada, S., Uezumi, A., Ikemoto, M., Masuda, S., Segawa, M., Tanimura, N., Yamamoto, H., Miyagoe-Suzuki, Y., and Takeda, S. (2007). Molecular signature of quiescent satellite cells in adult skeletal muscle. Stem Cells *25*, 2448–2459.

Gilbert, P.M., Havenstrite, K.L., Magnusson, K.E.G., Sacco, A., Leonardi, N.A., Kraft, P., Nguyen, N.K., Thrun, S., Lutolf, M.P., and Blau, H.M. (2010). Substrate elasticity regulates skeletal muscle stem cell self-renewal in culture. Science *329*, 1078–1081.

Gradilone, S.A., Radtke, B.N., Bogert, P.S., Huang, B.Q., Gajdos, G.B., and LaRusso, N.F. (2013). HDAC6 inhibition restores ciliary expression and decreases tumor growth. Cancer Res. *73*, 2259–2270.

Gray, J.V., Petsko, G.A., Johnston, G.C., Ringe, D., Singer, R.A., and Werner-Washburne, M. (2004). "Sleeping beauty": quiescence in Saccharomyces cerevisiae. Microbiol. Mol. Biol. Rev. *68*, 187–206.

Hausburg, M.A., Doles, J.D., Clement, S.L., Cadwallader, A.B., Hall, M.N., Blackshear, P.J., Lykke-Andersen, J., and Olwin, B.B. (2015). Post-transcriptional regulation of satellite cell quiescence by TTP-mediated mRNA decay. Elife *4*, e03390.

Hong, H., Kim, J., and Kim, J. (2015). Myosin heavy chain 10 (MYH10) is required for centriole migration during the biogenesis of primary cilia. Biochem. Biophys. Res. Commun. *461*, 180–185.

Huangfu, D., Liu, A., Rakeman, A.S., Murcia, N.S., Niswander, L., and Anderson, K.V. (2003). Hedgehog signalling in the mouse requires intraflagellar transport proteins. Nature *426*, 83–87.

Ikemoto, M., Fukada, S., Uezumi, A., Masuda, S., Miyoshi, H., Yamamoto, H., Wada, M.R., Masubuchi, N., Miyagoe-Suzuki, Y., and Takeda, S. (2007). Autologous transplantation of SM/C-2.6+ satellite cells transduced with micro-dystrophin CS1 cDNA by lentiviral vector into mdx mice. Mol. Ther. *15*, 2178–2185.

Jaafar Marican, N.H., Cruz-Migoni, S.B., and Borycki, A.-G. (2016). Asymmetric distribution of primary cilia allocates satellite cells for self-renewal. Stem Cell Rep. *6*, 798–805.

Jassal, B., Matthews, L., Viteri, G., Gong, C., Lorente, P., Fabregat, A., Sidiropoulos, K., Cook, J., Gillespie, M., Haw, R., et al. (2019). The reactome pathway knowledgebase. Nucleic Acids Res. *48*, D498–D503.

Johnson, K.A. (1998). The axonemal microtubules of the Chlamydomonas flagellum differ in tubulin isoform content. J. Cell Sci. *111*, 313–320.

Judson, R.N., and Rossi, F.M.V. (2020). Towards stem cell therapies for skeletal muscle repair. NPJ Regen. Med. *5*, 10.

Kanehisa, M. (2000). KEGG: kyoto encyclopedia of genes and genomes. Nucleic Acids Res. *28*, 27–30.

Kim, S., and Tsiokas, L. (2011). Cilia and cell cycle re-entry. Cell Cycle *10*, 2683–2690.

Lepper, C., Partridge, T.A., and Fan, C.-M. (2011). An absolute requirement for Pax7-positive satellite cells in acute injury-induced skeletal muscle regeneration. Development *138*, 3639–3646.

Liu, L., Cheung, T.H., Charville, G.W., and Rando, T.A. (2015). Isolation of skeletal muscle stem cells by fluorescence-activated cell sorting. Nat. Protoc. *10*, 1612–1624.

Liu, L., Charville, G.W., Cheung, T.H., Yoo, B., Santos, P.J., Schroeder, M., and Rando, T.A. (2018). Impaired notch signaling leads to a decrease in p53 activity and mitotic catastrophe in aged muscle stem cells. Cell Stem Cell *23*, 544–556.e4.

Mauro, A. (1961). Satellite cell of skeletal muscle fibers. J. Biophys. Biochem. Cytol. *9*, 493–495.

Montarras, D. (2005). Direct isolation of satellite cells for skeletal muscle regeneration. Science *309*, 2064–2067.

de Morrée, A., van Velthoven, C.T.J., Gan, Q., Salvi, J.S., Klein, J.D.D., Akimenko, I., Quarta, M., Biressi, S., and Rando, T.A. (2017). Staufen1 inhibits MyoD translation to actively maintain muscle stem cell quiescence. Proc. Natl. Acad. Sci. U S A *114*, E8996–E9005.

Motohashi, N., and Asakura, A. (2014). Muscle satellite cell heterogeneity and self-renewal. Front. Cell Dev. Biol. *2*, 1.

Olguin, H.C., and Olwin, B.B. (2004). Pax-7 up-regulation inhibits myogenesis and cell cycle progression in satellite cells: a potential mechanism for self-renewal. Dev. Biol. *275*, 375–388.

Palla, A.R., Hilgendorf, K.I., Yang, A.V., Kerr, J.P., Hinken, A.C., Demeter, J., Kraft, P., Mooney, N.A., Yucel, N., Jackson, P.K., et al. (2020). Ciliation of muscle stem cells is critical to maintain regenerative capacity and is lost during aging. bioRxiv https://doi.org/10.1101/2020.03.20.000943.

Pham, T.Q., Robinson, K., Xu, L., Skapek, S.X., and Chen, E.Y. (2019). HDAC6 promotes self-renewal and migration/invasion of rhabdomyosarcoma. bioRxiv https://doi.org/10.1101/823864.

Pugacheva, E.N., Jablonski, S.A., Hartman, T.R., Henske, E.P., and Golemis, E.A. (2007). HEF1-dependent Aurora A activation induces disassembly of the primary cilium. Cell *129*, 1351–1363.

Quarmby, L.M., and Parker, J.D.K. (2005). Cilia and the cell cycle? J. Cell Biol. *169*, 707–710.

Quarta, M., and Rando, T.A. (2015). Mimicking the niche: cytokines expand muscle stem cells. Cell Res. *25*, 761–762.

Quarta, M., Brett, J.O., DiMarco, R., De Morree, A., Boutet, S.C., Chacon, R., Gibbons, M.C., Garcia, V.A., Su, J., Shrager, J.B., et al. (2016). An artificial niche preserves the quiescence of muscle stem cells and enhances their therapeutic efficacy. Nat. Biotechnol. *34*, 752–759.

Rao, Y., Hao, R., Wang, B., and Yao, T.-P. (2014). A mec17-myosin II effector axis coordinates microtubule acetylation and actin dynamics to control primary cilium biogenesis. PLoS One *9*, e114087.

Relaix, F., and Zammit, P.S. (2012). Satellite cells are essential for skeletal muscle regeneration: the cell on the edge returns centre stage. Development *139*, 2845–2856.

Rinaldi, F., and Perlingeiro, R.C.R. (2014). Stem cells for skeletal muscle regeneration: therapeutic potential and roadblocks. Transl. Res. *163*, 409–417.

Sacco, A., Doyonnas, R., Kraft, P., Vitorovic, S., and Blau, H.M. (2008). Self-renewal and expansion of single transplanted muscle stem cells. Nature *456*, 502–506.

Sambasivan, R., Yao, R., Kissenpfennig, A., Van Wittenberghe, L., Paldi, A., Gayraud-Morel, B., Guenou, H., Malissen, B., Tajbakhsh, S., and Galy, A. (2011). Pax7-expressing satellite cells are indispensable for adult skeletal muscle regeneration. Development *138*, 3647–3656.

Scaramozza, A., Park, D., Kollu, S., Beerman, I., Sun, X., Rossi, D.J., Lin, C.P., Scadden, D.T., Crist, C., and Brack, A.S. (2019). Lineage tracing reveals a subset of reserve muscle stem cells capable of clonal expansion under stress. Cell Stem Cell *24*, 944–957.e5.

Schmidt, M., Schüler, S.C., Hüttner, S.S., von Eyss, B., and von Maltzahn, J. (2019). Adult stem cells at work: regenerating skeletal muscle. Cell. Mol. Life Sci. *76*, 2559–2570.

Seale, P., Sabourin, L.A., Girgis-Gabardo, A., Mansouri, A., Gruss, P., and Rudnicki, M.A. (2000). Pax7 is required for the specification of myogenic satellite cells. Cell *102*, 777–786.

Sirajuddin, M., Rice, L.M., and Vale, R.D. (2014). Regulation of microtubule motors by tubulin isotypes and post-translational modifications. Nat. Cell Biol. *16*, 335–344.

Subramanian, A., Tamayo, P., Mootha, V.K., Mukherjee, S., Ebert, B.L., Gillette, M.A., Paulovich, A., Pomeroy, S.L., Golub, T.R., Lander, E.S., et al. (2005). Gene set enrichment analysis: a knowledge-based approach for interpreting genome-wide expression profiles. Proc. Natl. Acad. Sci. U S A *102*, 15545–15550.

Tang, A.H., and Rando, T.A. (2014). Induction of autophagy supports the bioenergetic demands of quiescent muscle stem cell activation. EMBO J. *33*, 2782–2797.

Tao, H., Chen, Y., Sun, Z., Chen, H., and Chen, M. (2018). Silence of HDAC6 suppressed esophageal squamous cell carcinoma proliferation and migration by disrupting chaperone function of HSP90. J. Cell. Biochem. *119*, 6623–6632.

Tucker, R.W., Pardee, A.B., and Fujiwara, K. (1979a). Centriole ciliation is related to quiescence and DNA synthesis in 3T3 cells. Cell *17*, 527–535.

Tucker, R.W., Scher, C.D., and Stiles, C.D. (1979b). Centriole deciliation associated with the early response of 3T3 cells to growth factors but not to SV40. Cell *18*, 1065–1072.

Valcourt, J.R., Lemons, J.M.S., Haley, E.M., Kojima, M., Demuren, O.O., and Coller, H.A. (2012). Staying alive: metabolic adaptations to quiescence. Cell Cycle *11*, 1680–1696.

Der Vartanian, A., Quétin, M., Michineau, S., Auradé, F., Hayashi, S., Dubois, C., Rocancourt, D., Drayton-Libotte, B., Szegedi, A., Buckingham, M., et al. (2019). PAX3 confers functional heterogeneity in skeletal muscle stem cell responses to environmental stress. Cell Stem Cell *24*, 958–973.e9.

van Velthoven, C.T.J., and Rando, T.A. (2019). Stem cell quiescence: dynamism, restraint, and cellular idling. Cell Stem Cell *24*, 213–225.

Webster, M.T., Manor, U., Lippincott-Schwartz, J., and Fan, C.-M. (2016). Intravital imaging reveals ghost fibers as architectural units guiding myogenic progenitors during regeneration. Cell Stem Cell *18*, 243–252.

White, J.P., Billin, A.N., Campbell, M.E., Russell, A.J., Huffman, K.M., and Kraus, W.E. (2018). The AMPK/p27Kip1 Axis regulates autophagy/apoptosis decisions in aged skeletal muscle stem cells. Stem Cell Reports *11*, 425–439.

Woan, K.V., Lienlaf, M., Perez-Villaroel, P., Lee, C., Cheng, F., Knox, T., Woods, D.M., Barrios, K., Powers, J., Sahakian, E., et al. (2015). Targeting histone deacetylase 6 mediates a dual anti-melanoma effect: enhanced antitumor immunity and impaired cell proliferation. Mol. Oncol. *9*, 1447–1457.

Zitouni, S., Francia, M.E., Leal, F., Montenegro Gouveia, S., Nabais, C., Duarte, P., Gilberto, S., Brito, D., Moyer, T., Kandels-Lewis, S., et al. (2016). CDK1 prevents unscheduled PLK4-STIL complex assembly in centriole biogenesis. Curr. Biol. *26*, 1127–1137.

Stem Cell Reports, Volume *17*

Supplemental Information

Tubastatin A maintains adult skeletal muscle stem cells in a quiescent state *ex vivo* and improves their engraftment ability *in vivo*

Marina Arjona, Armon Goshayeshi, Cristina Rodriguez-Mateo, Jamie O. Brett, Pieter Both, Heather Ishak, and Thomas A. Rando

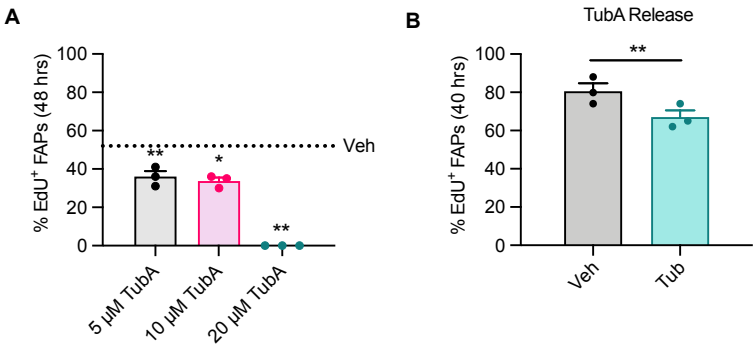
A
% EdU+ FAPs (48 hrs)
100
80
60
40
20
0
Veh
**
*
**
5 μM TubA
10 μM TubA
20 μM TubA
B
TubA Release
% EdU+ FAPs (40 hrs)
100
80
60
40
20
0
**
Veh
Tub

Figure S1

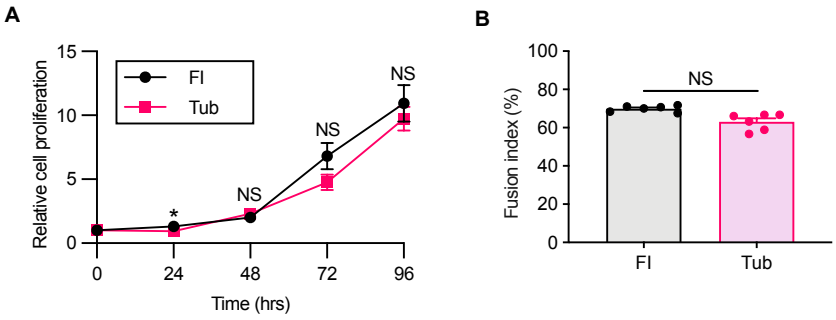
A
B
Relative cell proliferation
Time (hrs)
FI
Tub
NS
NS
NS
*
Fusion index (%)
NS
FI
Tub

Figure S2

Supplemental Figure Legends

Figure S1. TubA prevents FAP entry into the cell cycle. A, FACS-isolated FAPs were treated with different doses of TubA for 48 hrs while being cultured continuously in EdU to assess S-phase progression. The percentage of EdU+ FAPs was quantified (*n*= 3 mice). **B**, FAPs were cultured in the absence or presence of 20 μM of TubA for 48 hrs. Cells were then cultured for 40 hrs in the absence of TubA but the presence of EdU, after which the number of EdU+ FAPs was quantified (*n*=3 mice). Error bars represent ± s.e.m. *P <0.05, **P<0.01; two-tailed paired t-test.

Figure S2. *In vitro* proliferation and differentiation characteristics of TubA-released MuSCs are comparable to those of MuSCs^{FI}. A, FACS-isolated MuSCs were cultured in the presence of TubA for 72 hrs, then released from TubA and maintained in culture for 96 hrs. Cells were fixed at the moment of TubA release (0 hrs) or 24, 48, 72, and 96 hrs after TubA release. As a control, FACS-isolated MuSCs were grown in culture for 96 hrs. The number of MuSCs at each time point was quantified (*n*=12 mice). **B**, FACS-isolated MuSCs were cultured in the presence of TubA for 72 hrs, then released from TubA and cultured in wash media for 48 hrs. Cells were then cultured in differentiation media for another 48 hrs. As a control, FACS-isolated MuSCs were grown in wash media for 48 hrs and then in differentiation media for another 48 hrs. Myonuclear fusion index was measured as the percentage of DAPI+ nuclei from each well that were within MHC+ myotubes that contained more than one nucleus (*n*= 6 mice). Error bars represent ± s.e.m. *P <0.05; NS: not significant; two-tailed t-test.

Supplemental Experimental Procedures

EdU assay. To analyze S-phase entry of MuSCs *ex vivo*, FACS-isolated MuSCs were cultured in the presence of 10 μM EdU (Thermo Fisher) for different periods of time (indicated in each experiment). Cells were fixed with 4% PFA for ten minutes, permeabilized using 0.5% Triton in PBS, and blocked using 3% BSA in PBS. Cells were then stained with the Click-iT EdU Cell Proliferation Kit (Thermo Fisher) and DAPI. The percentage of EdU^+ cells was quantified automatically using the Volocity software.

Cell size, Pyronin Y, and Annexin V assays. To assess cell size, RNA content, and cell survival, MuSCs cells were cultured in growth media (Ham's F-10 media containing 20% fetal bovine serum, 2.5 ng/mL bFGF (PeproTech), 100 U/mL penicillin, and 100 μg/mL streptomycin). At various time-points after plating (indicated in each experiment), cells were trypsinized using TrypLE Select (Thermo Fisher). To test cellular diameter, cells were assayed with a Moxi Flow combined Coulter counter and flow cytometer (Orflo Technologies). For RNA content, MuSCs were blocked for forty-five minutes at 37°C with wash media, and 10 μM Hoechst 33342 (Thermo Fisher), and then stained with 0.1 mg/mL Pyronin Y (Santa Cruz sc-203755) for fifteen minutes at 37°C in the same medium. To assess for cell survival, detached cells were collected and pooled with attached cells after gentle detachment with TrypLE Select. Cells were then stained with an Annexin V antibody (BioLegend) and with Propidium Iodide (BioLegend) for ten minutes at 4°C. Each analysis was done with 1000 cells using an Aria II or Aria III machine. Cell size was recorded in the FSC-A channel, pyronin Y intensity in the PE-Cy5 channel, and Annexin V signal in the FITC channel.

Differentiation assay. To assess differentiation, freshly-isolated MuSCs were grown in wash media for 48 hrs and then in differentiation media (DMEM media containing 5% horse serum, 100 U/mL penicillin, and 100 μg/mL streptomycin) for another 48 hrs. To examine the differentiation capacity of TubA-released MuSCs, freshly-isolated MuSCs were cultured in the presence of TubA for 72 hrs. TubA was then washed out and cells were cultured in wash media for 48 hrs. Next, cells were grown in differentiation media for another 48 hrs. Myonuclear fusion index was measured as the percentage of DAPI+ nuclei from each well that were within MHC+ myotubes that contained more than one nucleus. Myonuclear fusion index was quantified from immunofluorescent DAPI and MHC images using the thresholding and contour functions (adaptiveThreshold, findContours, contourArea, and arcLength) of the open source Python package, OpenCV (https://pypi.org/project/opencv-python/), and the Image.getpixel function of the open source Python Imaging Library (https://pypi.org/project/Pillow/).

Immunofluorescence assay. To examine MyoD, Pax7, Ift20, Arl13b, or detyrosinated tubulin (detyr-tub) expression, MuSCs were fixed with 4% formaldehyde for ten minutes, permeabilized with 0.2% Triton X-100 in PBS for another ten minutes, blocked in PBS containing 10% FBS, 1% BSA, 0.1% Tx100 and 0.01% NaN_3 for 60 minutes, and then stained with antibodies against MyoD (1:100, BD 554130), Pax7 (1:50, DSHB AB_528428), Ift20 (1:1000, Sigma-Aldrich HPA021376), Arl13b (1:1000, NeuroMab clone N295B/66) or detyr-tub (1:500, Abcam ab48389) overnight at 4°C. Nuclei were stained with DAPI. The fraction of $MyoD^+$ cells, $Pax7^+$ cells, $Ift20^+$ cells, $Arl13b^+$ cells, and detyr-tub+ cells was quantified using Volocity software. To analyze Pax7 expression levels, $DAPI^+$ nuclear regions were identified automatically using the contour functions (findContours, contourArea, and arcLength) of the OpenCV2 Python library,

and mean fluorescence intensity of the Pax7 channel was calculated using the Image.getpixel() command from the Python Imaging Library and the np.mean() command from the NumPy Library.

Muscle injury. For transplantation experiments, lower hindlimbs of NSG mice were anesthetized with isoflurane and tibialis anterior (TA) muscles were injured with 40 μL of 1.2% barium chloride (Sigma) injected over fifteen intramuscular pokes. TA muscles from recipient mice were injured 72 hrs before transplantation.

MuSC transplantation and tamoxifen treatment. In order to label MuSCs with RFP, $Pax7^{CreER}$; $Rosa26R^{RFP}$ mice received tamoxifen (Sigma) at 80 mg/kg in 100% corn oil. Tamoxifen was delivered via intraperitoneal injection for seven consecutive days. After tamoxifen injections, a chase period of two weeks was given to the mice before any experiment was performed. MuSCs were then isolated based on RFP expression via FACS. RFP+ MuSCs were maintained in culture in the presence of either TubA or DMSO for 72 hrs before being used as donors. RFP+ MuSCs were trypsinized using TrypLE Select (Thermo Fisher) and resuspended in PBS before transplantation. Twenty-thousand cells were suspended in 40 μL of PBS and injected into injured TA muscles of recipient NSG mice. Either ten days or four weeks after transplantation, the mice were sacrificed, and their muscles were analyzed.

In the experiments where TubA was added to cycling MuSCs, freshly isolated RFP+ MuSCs were expanded for 72 hrs in growth media and then treated with either TubA or DMSO for 48 hrs in wash media before transplantation. RFP+ MuSCs were trypsinized using TrypLE Select and resuspended in PBS before transplantation. Twenty-thousand cells were suspended in 40 μL

of PBS and injected into injured TA muscles of recipient NSG mice. Ten days after transplantation, the mice were sacrificed and their muscles were analyzed.

Bioluminescence (BLI) imaging. For BLI experiments, mice were anaesthetized using isoflurane and intraperitoneally injected with d-Luciferin (50 mg/ml, Biosynth International Inc.). Immediately after the injection, mice were imaged using the Xenogen IVIS-Spectrum System (Caliper Life Sciences). Images were taken every minute using medium binning, maximum sensitivity (f-stop 1) and a 1 min exposure time. Imaging was performed until the bioluminescent signal reached saturation. Living Image Software (Caliper Life Sciences) was then used to analyze the images obtained. For the analysis, a small region of interest (ROI) was generated and used in every transplanted TA muscle.

Histology. To test for MuSC engraftment ability in transplantation experiments, muscles were fixed with 0.5% formaldehyde for six hours, cryoprotected with 20% sucrose overnight, and then fresh-frozen in liquid nitrogen cooled isopentane. Transverse 10 μm cryosections were collected and fixed with 2% formaldehyde for ten minutes. The muscles were then stained for laminin using a rat anti-laminin α2 antibody (1.5 μg/mL, Abcam ab11576) for 2 hrs. DNA was stained with DAPI. Images from the entire section were taken and the number of RFP+ myofibers was manually quantified using Volocity software.

RNA-Seq. Freshly isolated MuSCs or MuSCs grown *ex vivo* for 24 hrs in the presence of either DMSO or TubA were snap-frozen, and total RNA was extracted using the RNeasy Micro Plus Kit (Qiagen) according to manufacturer's instructions. Reverse transcription was performed with

5 ng RNA using the SMART-Seq v4 Ultra Low Input RNA Kit (Takara). The cDNA was then sheared with a Covaris S2 ultrasonicator and library constructions were performed using the Ovation Ultralow Multiplex system (NuGEN). Libraries underwent paired-end 150-bp sequencing at Novogene with an Illumina HiSeq 2000 to a depth of 20-40 million reads.

RNAseq reads were processed with trim_galore for quality and adapter removal (www.bioinformatics.babraham.ac.uk/projects/trim_galore). Reads were then mapped to the mouse genome (mm10) with Ensembl transcript annotations using (Dobin et al., 2013). Uniquely mapping exonic reads were summarized over genes with the featureCounts module of Subread (Liao et al., 2014). Counts were analyzed using edgeR (Robinson et al., 2010), normalizing with the Trimmed Mean of M-values method and performing differential expression testing with Cox-Reid estimations of tagwise dispersions and the negative binomial GLM likelihood ratio test. The Benjamini-Hochberg method was used to generate false discovery rates.

Gene expression heatmaps were generated in R using the pheatmap package. Mean group FPKM values were log2-transformed for color mapping, and genes were clustered by Manhattan distance and single linkage.

Genes were analyzed with GSEA (Subramanian et al., 2005) using the MSigDB Hallmark gene sets (Liberzon et al., 2015) (enrichment statistic p 1, ranking metric Signal2Noise, expressed gene set size range 15-500). For overrepresentation analysis (ORA), fold-change <2 and Benjamini-Hochberg-corrected p-value >0.05 were used to classify genes as "similar" between $MuSCs^{FI}$ and $MuSCs^{Tub}$. FDR 1% was used to identify genes that were significantly different between $MuSCs^{FI}$ and $MuSCs^{Veh}$ as well as between $MuSCs^{Tub}$ and $MuSCs^{Veh}$. The REACTOME and KEGG pathway databases were used to annotate genes.

RT-qPCR. Total RNA was extracted using the RNeasy Plus Micro Kit (Qiagen) and reverse transcribed using the High-Capacity cDNA Reverse Transcription Kit (Applied Biosystems). Quantitative PCR was performed with the LightCycler 480 I SYBR Green PCR Master Mix (Roche). Each measurement was performed in triplicate and the values were averaged and normalized to *Gapdh*. Relative expression was calculated using the comparative CT method (Pfaffl, 2001). RT-qPCR primer sequences were, from 5' to 3':

Cyclin D1: AGACCATTCCCTTGACTGC, AAGCAGTTCCATTTGCAGC

Cyclin-dependent kinase 1: GTCCGTCGTAACCTGTTGAG,

TGACTATATTTGGATGTCGAAG

Polo like kinase 4: AGGAGAAACTAATGAGCACCACA, TGGCTCTCGTGTCAGTCCAA

GLI-Kruppel family member GLI3: AAGCGGTCCAAGATCAAGC,

TGTTCCTTCCGGCTGTTC

Smoothened: AGAGCAAGATGATCGCCAAG, CCATCATGGGAGACAGTGTG

Gapdh: GACTTCAACAGCAACTCCCAC, TCCACCACCCTGTTGCTGTA

Statistics. When data are summarized using a column with individual data points, each data point represents a biological replicate and error bars represent s.e.m. In time series graphs each data point represents the mean and the error bars represent s.e.m. Significance was calculated using two-tailed *t*-tests, except in the RT-qPCR experiments in which one tailed *t*-tests were performed. Differences were considered to be statistically significant at the $P < 0.05$ level.

Supplemental References

Dobin, A., Davis, C.A., Schlesinger, F., Drenkow, J., Zaleski, C., Jha, S., Batut, P., Chaisson, M., and Gingeras, T.R. (2013). STAR: ultrafast universal RNA-seq aligner. Bioinformatics *29*.

Liao, Y., Smyth, G.K., and Shi, W. (2014). featureCounts: an efficient general purpose program for assigning sequence reads to genomic features. Bioinformatics *30*.

Pfaffl, M.W. (2001). A new mathematical model for relative quantification in real-time RT-PCR. Nucleic Acids Res. *29*.

Robinson, M.D., McCarthy, D.J., and Smyth, G.K. (2010). edgeR: a Bioconductor package for differential expression analysis of digital gene expression data. Bioinformatics *26*.